Articles

Identification of Amino Acids in the Nicotinic Acetylcholine Receptor Agonist Binding Site and Ion Channel Photolabeled by 4-[(3-Trifluoromethyl)-3*H*-Diazirin-3-yl]Benzoylcholine, a Novel Photoaffinity Antagonist†

David C. Chiara, Jonathan C. Trinidad, Dong Wang, Michael R. Ziebell, Deirdre Sullivan, and Jonathan B. Cohen*

Department of Neurobiology, Harvard Medical School, Boston, Massachusetts 02115

Received October 10, 2002; Revised Manuscript Received November 18, 2002

ABSTRACT: [^{3}H]4-[(3-trifluoromethyl)-3*H*-diazirin-3-yl]benzoylcholine (TDBzcholine) was synthesized and used as a photoaffinity probe to map the orientation of an aromatic choline ester within the agonist binding sites of the *Torpedo* nicotinic acetylcholine receptor (nAChR). TDBzcholine acts as a nAChR competitive antagonist that binds at equilibrium with equal affinity to both agonist sites ($K_D \sim 10$ μM). Upon UV irradiation (350 nm), nAChR-rich membranes equilibrated with [^{3}H]TDBzcholine incorporate ^{3}H into the α, γ, and δ subunits in an agonist-inhibitable manner. The specific residues labeled by [^{3}H]TDBzcholine were determined by N-terminal sequence analysis of subunit fragments produced by enzymatic cleavage and purified by sodium dodecyl sulfate-polyacrylamide gel electrophoresis and/or reversed-phase high-performance liquid chromatography. For the α subunit, [^{3}H]TDBzcholine photoincorporated into αCys-192, αCys-193, and αPro-194. For the γ and δ subunits, [^{3}H]TDBzcholine incorporated into homologous leucine residues, γLeu-109 and δLeu-111. The photolabeling of these amino acids suggests that when the antagonist TDBzcholine occupies the agonist binding sites, the Cys-192-193 disulfide and Pro-194 from the α subunit Segment C are oriented toward the agonist site and are in proximity to γLeu-109/δLeu-111 in Segment E, a conclusion consistent with the structure of the binding site in the molluscan acetylcholine binding protein, a soluble protein that is homologous to the nAChR extracellular domain.

Nicotinic acetylcholine receptors (nAChR)[1] are ligand-gated ion channels that are allosterically activated by the neurotransmitter acetylcholine (ACh). nAChRs of vertebrate skeletal muscle and the electric organs of a marine ray, *Torpedo*, are made up of four homologous subunits ($\alpha_2\beta\gamma\delta$) that are arranged pseudosymmetrically about a central axis that is a cation-selective ion channel. Each nAChR contains two ACh binding sites that are located in the extracellular domain at the interfaces between the α and γ subunits and the α and δ subunits, and agonist binding to both sites is required to open the channel. Affinity-labeling and mutagenesis studies provide extensive evidence that the amino acids contributing to the ACh sites are from three distinct regions of the α subunit primary structure [referred to as binding-site Segments A (α93), B (α149), and C (α190−200)] and from three or more regions of the γ/δ subunits [D (γ55−59), E (γ109−119), and F (amino acids distributed between γ161 and γ180)] (reviewed in refs *1*−*3*).

Recently, a molluscan ACh binding protein (AChBP) was isolated that is a secreted, soluble, homopentameric homologue of the N-terminal, extracellular domain of a nAChR (*4*). The determination of its crystal structure at atomic resolution (2.7 Å) (*5*) provides a general description of the extracellular domain and transmitter binding site for nAChRs as well as all other members of this ligand-gated ion channel superfamily including the $GABA_A$, glycine, and serotonin $5HT_3$ receptors. Even though the AChBP was crystallized in the absence of agonist, the transmitter binding sites were easily recognized by reference to the nAChR binding-site amino acids previously identified by affinity labeling and mutational analyses. The amino acids equivalent to *Torpedo* nAChR αTyr-93, αTrp-149, αTyr-190, αCys-192/193, αTyr-198, and γTrp-55/δTrp-57 are all conserved in the AChBP,

† This research was supported in part by USPHS Grants NS 19522 and GM 58448 and by awards to Harvard Medical School in Structural Neurobiology from the Keck Foundation and from the Howard Hughes Medical Institute Biomedical Research Support Program for Medical Schools.

* To whom correspondence should be addressed: Tel: (617) 432-1728. Fax: (617) 734-7557. E-mail: jonathan_cohen@hms.harvard.edu.

[1] Abbreviations: nAChR, nicotinic acetylcholine receptor; ACh, acetylcholine; AChBP, acetylcholine binding protein from *Lymnaea stagnalis*; Bz_2choline, 4-benzoylbenzoylcholine; TDBzcholine, 4-[(3-trifluoromethyl)-^{3}H-diazirin-3-yl]benzoylcholine; Carb, carbamylcholine chloride; CDI, 1,1-carbonyl diimidazole; DMF, *N*,*N*-dimethylformamide; TDBz acid, 4-(1-Azi-2,2,2-trifluoroethyl)benzoic acid; V8 protease, *Staphylococcus aureus* glutamyl endopeptidase; EndoLys-C, endoproteinase Lys-C; EndoAsp-N, endoproteinase Asp-N; Endo H, Endoglycosidase H; α-BgTx, αBungarotoxin; [^{125}I]TID, 3-(trifluoromethyl)-3-(*m*-[^{125}I]iodophenyl)diazirine; HTX, Perhydrohistrionicotoxin; TPS, *Torpedo* physiological saline; dTC, D-tubocurarine; SDS, sodium dodecyl sulfate; PAGE, polyacrylamide gel electrophoresis; HPLC, high-performance liquid chromatography;.

10.1021/bi0269815 CCC: $25.00
Published on Web 12/21/2002

with the five aromatic side chains organized to form a well-defined binding pocket at each of the subunit interfaces in a position that would be ~30 Å above the bilayer in a nAChR. The side chains identified in *Torpedo* or muscle nAChR Segment E that interact with antagonists (*6*−*10*) are not conserved in the AChBP, but the positions relative to the conserved γGly-114 all lie on the common surface of antiparallel β-strands that form part of the entry to the binding pocket. There is no evidence that the AChBP exists in more than one conformation, and comparison of its structure with that of the *Torpedo* nAChR structure at 4.7 Å resolution indicates that the structure of the AChBP binding site is closer to that of a nAChR in a conformation that binds ACh with high affinity (open channel or desensitized states) than with low affinity (closed channel) (*11*).

Affinity labeling and mutational analyses are beginning to provide information about the orientation of quaternary ammonium agonists and antagonists bound within the ACh site. Bromoacetylcholine acts as a covalent agonist when tethered at αCys-192/193 in reduced, wild-type nAChR (*12*, *13*), while thiocholine acts as a covalent agonist when tethered at αTyr198Cys (*14*). The introduction of unnatural amino acids within the binding site by use of the in vivo nonsense-suppression method has provided evidence that nAChR activation depended especially upon interactions of the cationic quaternary ammonium of ACh with the indole side chain of αTrp-149 (*15*). For the nAChR in the desensitized state, the selective reaction of [^{3}H]acetylcholine mustard with αTyr-93 provides evidence that this amino acid interacts with the quaternary ammonium (*16*), while the ester moiety of ACh is predicted to be oriented toward αTyr-190/αCys-192/193 since they are photolabeled by the agonist [^{3}H]-(diazocyclohexadienoylpropyl)trimethylammonium (*17*). In addition, [^{3}H]4-benzoylbenzoylcholine (Bz_2choline), an nAChR antagonist that contains a photoreactive ketone ~10 Å from the quaternary ammonium, was photoincorporated selectively into the homologous residues γLeu-109 and δLeu-111, with no significant incorporation within the α subunit (*10*).

To further define the structure of the nAChR agonist site and the orientation of bound aromatic choline esters site, we introduce in this report [^{3}H]4-(1-azi-2,2,2-trifluoromethyl)benzoylcholine (TDBzcholine), which contains a photoreactive diazirine in the para-position. The mechanism of photoreactivity of TDBzcholine, which forms a reactive carbene upon UV irradiation, is quite different than that of the ketyl diradical formed by Bz_2choline (*18*), and we wanted to determine whether the TDBzcholine would react similarly with γLeu-109/δLeu-111 or whether it would identify additional amino acids in proximity to the para-position of benzoylcholine.

EXPERIMENTAL PROCEDURES

Materials. nAChR-rich membranes were isolated from the electric organs of *Torpedo californica* (Winkler Enterprises, San Pedro, CA) as described previously (*19*), and the final membrane suspensions were stored under argon in 36% sucrose/0.02% sodium azide at −80 °C. Choline *p*-toluenesulfonate, diisopropylphosphofluoridate, carbamylcholine chloride (Carb), 1,1-carbonyl diimidazole (CDI), and *N*,*N*-dimethylformamide (DMF) were purchased from Sigma-Aldrich. 4-(1-azi-2,2,2-trifluoroethyl)benzoic acid (TDBz acid) was purchased from Bachem (Q-1540). *Staphylococcus aureus* glutamyl endopeptidase (V8 protease) was purchased from ICN Biomedicals. Endoproteinase Lys-C (EndoLys-C) and Endoproteinase Asp-N (EndoAsp-N) were obtained from Roche Biochemical. *S. plicatus* endoglycosidase H (Endo H) was from Glyko. Prestained low molecular mass gel standards were from Life Technologies, Inc. (in kDa: ovalbumin, 43; carbonic anhydrase, 29; β-lactoglobin, 20; lysozyme, 14; bovine trypsin inhibitor, 5.5; and insulin, 2.8). (3-[^{125}I]iodotyrosyl^{54})-α-bungarotoxin (150 Ci/mmol, [^{125}I]α-BgTx) and [methyl-^{3}H]choline chloride (85 Ci/mmol) were from Amersham Pharmacia Biotech and American Radiolabeled Chemicals, respectively, and [^{3}H]ACh (5.5 Ci/mmol) was kindly provided by Dr. Keith Miller (Massachusetts General Hospital). [^{3}H]Perhydrohistrionicotoxin (HTX) (12 Ci/mmol) was prepared from D,L-decahydro(pentenyl)histrionicotoxin by catalytic tritiation using carrier-free tritium gas (NEN Life Science Products). Aluminum-backed, high-performance thin-layer chromatography plates and glass-backed, preparative plates (silica gel, 60 F 254) were from Merck.

Synthesis of TDBzcholine. TDBzcholine was synthesized by coupling TDBz acid to choline chloride with CDI. TDBz acid (20 mg, 0.09 mmol) was dissolved in 2 mL of anhydrous DMF to which was added CDI (25 mg, 0.15 mmol). The reaction was stirred at room temperature in the dark for 40 min before addition of dry choline chloride (30 mg, 0.22 mmol). Choline chloride was partially soluble in DMF, and over time, most dissolved. After overnight reaction, the mixture was applied to a Vydac C18 semipreparative column and eluted over 50 min with a gradient of acetonitrile from 0−75% with 0.02% acetic acid present in both buffers. Free choline eluted with the flow-through, while TDBzcholine eluted as a broad peak around 40% acetonitrile. The peaks from three separate HPLC runs were pooled and dried by rotary evaporation. This material was resolubilized in 100% D_2O, and the concentration was determined by absorption at 348 nm ($\epsilon = 369$). The yield was 50% based on absorption.

The structure and purity were verified by thin-layer chromatography, NMR, and mass spectrometry. When characterized on a silica gel plate with the chromatogram developed in a solvent mixture made up of chloroform/methanol/acetic acid (1:2:0.1, v/v/v), TDBzcholine migrated as a single spot ($R_f = 0.3$) well-separated from the position of migration of TDBz acid ($R_f = 0.95$). When TDBzcholine acetate in 100% D_2O was characterized by ^{1}H NMR (200 MHz), the following spectrum was observed: 7.9 ppm (d, 2 H), 7.25 ppm (d, 2 H), 4.77 ppm (m, 2 H), 3.75 ppm (t, 2 H), 3.15 ppm (s, 9 H). In addition, there was a peak at 1.8 ppm (s, 3 H) originating from the methyl protons from the acetate salt. Electrospray ionization mass spectrometry using a Finnegan LCQ Deca with an ESI probe revealed a primary mass fragment ($m/z = 316$ (exact 316.1 M^+)) with a fragmentation pattern consistent with the expected product.

[^{3}H]TDBzcholine was synthesized at a radiochemical specific activity of 0.6 Ci/mmol. 5.3 mCi of [methyl-^{3}H]-choline chloride (85 Ci/mmol, 0.06 μmol) in 5 mL of ethanol was added to 2.3 mg of choline *p*-toluenesulfonate (8.4 μmol) and then dried. TDBz acid (13.6 mg, 5.9 μmol) was combined with CDI (12 mg, 74 μmol) in 150 μL of DMF and stirred at room temperature for 4 h. This was then added

to the dry [methyl-^{3}H]choline *p*-toluenesulfonate and reacted overnight at room temperature in the dark. The reaction mixture was loaded on an aluminum-backed silica thin layer plate (20 × 20 cm) and developed in 5:10:1 chloroform/methanol/acetic acid for 5 h. The product was located by UV fluorescence (254 nm, brief exposure). The strip containing the product was cut out, and [^{3}H]TDBzcholine was eluted in 10 mL of 50% methanol/H_2O (72 h, 3 °C). The eluate was filtered through a Buchner funnel, and the volume was reduced to 1 mL by centrifugal vacuum evaporation. A yield of 80% was calculated based on the absorbance at 348 nm.

Electrophysiology. Standard two-electrode voltage clamp techniques were used as described (*20*) to characterize the agonist/antagonist properties of TDBzcholine interacting with wild-type *Torpedo* nAChRs expressed in *Xenopus* oocytes.

Radioligand Binding Assays. The equilibrium binding of radioactive cholinergic ligands to nAChR-rich membranes in *Torpedo* physiological saline (TPS; 250 mM NaCl, 5 mM KCl, 3 mM $CaCl_2$, 2 mM $MgCl_2$, and 5 mM $NaPO_4$, pH 7.0) was measured by centrifugation in a Tomy MXT-150 microcentrifuge (*21*). Suspensions were pretreated with diisopropylphosphofluoridate (~0.5 mM) to inhibit esterase activity. For [^{3}H]ACh (30 nM), binding was measured using dilute membrane suspensions (1 mL, 70 μg protein/mL and 20 nM [^{3}H]ACh sites). Binding of [^{3}H]HTX (100 nM) was measured at 0.3 mg protein/mL (200 μL). Binding of [^{3}H]-TDBzcholine was measured at 1.0 mg protein/mL (100 μL, 1 μM [^{3}H]ACh sites). Membrane suspensions were equilibrated with drugs for 1 h before centrifugation, with the exception of [^{3}H]HTX, which was incubated for 2 h. Nonspecific binding of [^{3}H]ACh and [^{3}H]TDBzcholine was determined in the presence of 1 mM Carb and that of [^{3}H]-HTX in the presence of 30 μM proadifen. The effects of TDBzcholine or D-tubocurarine (dTC) on the initial rates of [^{125}I]α-BgTx binding to nAChR-rich membranes in TPS were determined by a centrifugation assay as described (*10*).

Data Analysis. The concentration-dependence of TDBzcholine inhibition of ACh-induced currents, radioligand binding, or subunit photolabeling was fit to

$$f(x) = f_0/[1 + (x/IC_{50})^n] + f_{ns} \quad (1)$$

where $f(x)$ is the current, total radioligand binding, or subunit incorporation of ^{3}H measured in the presence of inhibitor concentration x; f_0 is the current, specific binding, or specific subunit photolabeling in the absence of inhibitor; IC_{50} is the TDBzcholine concentration associated with 50% inhibition; n is the Hill coefficient; and f_{ns} is the leak current in the absence of ACh, the nonspecific radioligand binding, or the nonspecific subunit photolabeling. The concentration-dependent inhibition of the initial rate of [^{125}I]α-BgTx binding by TDBzcholine or dTC was fit according eq 1 and also, for dTC, to a two-site model as shown in

$$f(x) = 0.5f_0/[1 + (x/K_H)] + 0.5f_0/[1 + (x/K_L)] \quad (2)$$

where $f(x)$ is the initial rate of [^{125}I]α-BgTx binding seen in the presence of inhibitor concentration x, f_0 is the rate of binding in the absence of inhibitor, and K_H and K_L are the dissociation constants for the high- and low-affinity binding sites, respectively. Equilibrium binding data for [^{3}H]TDBzcholine were fit to a single-site model with a linear, nonspecific binding component as shown in

$$B(x) = B_{max}/[1 + (K_{eq}/x)] + m \cdot x \quad (3)$$

where $B(x)$ is the [^{3}H]TDBzcholine bound at a free concentration x, B_{max} is the concentration of [^{3}H]TDBzcholine binding sites, K_{eq} is the dissociation constant, and m is the slope of nonspecific binding derived from parallel experiments performed in the presence of 1 mM Carb. SigmaPlot (SPSS) was used for nonlinear least-squares fit of the data, and the standard errors of the parameter fits are indicated.

Photolabeling of nAChR-Rich Membranes with [^{3}H]-TDBzcholine. Membrane suspensions (3 mg protein/mL) in TPS were incubated with 0.5 mM diisopropylphosphofluoridate for 60 min to inactivate acetylcholinesterase prior to addition of [^{3}H]TDBzcholine. For labeling on an analytical scale, 75−100 μL aliquots in 96 well plastic microtiter plates were equilibrated at room temperature with [^{3}H]TDBzcholine and additional cholinergic ligands for 20 min prior to photolysis, except for α-BgTx, which was incubated with the membranes for 60 min prior to addition of [^{3}H]-TDBzcholine. The samples were irradiated on ice for 30 min using either a 365-nm handheld lamp (Spectroline EN16) at a distance of 6 cm or in a Rayonet RPR-200 photochemical reactor (Southern New England Ultraviolet) equipped with 3500-Å lamps. Polypeptides were resolved by SDS−PAGE and visualized by Coomassie blue stain. To determine the relative amount of [^{3}H]TDBzcholine photoincorporation into individual fragments, bands of interest were either excised and counted in gel cocktail as described previously (*22*) or the gel was treated with Amplify (Amersham) and exposed for fluorography.

For labeling on a preparative scale, membrane suspensions (3 mg/mL; 3−7 mL in 2.5 cm diameter plastic Petri dishes) were equilibrated with [^{3}H]TDBzcholine (15 μM) and 30 μM proadifen, a desensitizing aromatic amine noncompetitive antagonist (*23*). After photolysis, membrane polypeptides were separated by SDS−PAGE and then visualized by GelCode stain (Pierce). The nAChR subunits were excised and either passively eluted as described (*10*) or further digested with *S. aureus* V8 protease in a second mapping gel as described (*24*). Polypeptide bands in the mapping gel were visualized by Coomassie blue stain, excised, and passively eluted. The eluates were filtered (Whatman No. 1 filter paper), and the protein was concentrated to ~200 μL with Ultrafree-15 centrifugal filter devices with Biomax-5 cutoff filters (Millipore). Excess SDS was removed by acetone precipitation (75% final concentration, >2 h at −20 °C). Starting from 15 mg of nAChR-rich membranes (typically ~15 nmol ACh sites), 300−500 μg of protein was recovered from the eluates of nAChR subunit bands. As noted previously (*25*), based upon N-terminal sequence analyses, the nAChR γ and δ subunit preparations both contained as a major contaminant the β subunit of the Na^+/K^+-ATPase, which was present at 30−100% the level of the γ or δ subunit.

Enzymatic Digestions and Peptide Purification. For solution digestion with V8 protease, nAChR subunits or subunit fragments were resuspended in phosphate digestion buffer (10 mM sodium phosphate, pH 7.0, 1 mM dithiothreitol, 1 mM ethylenediamine-tetraacetic acid, and 0.1% SDS) with V8 protease (20% w/w). For digestion with EndoLys-C,

nAChR subunits were resuspended in 25 mM Tris, pH 8.6 (with 0.5 mM ethylenediamine-tetraacetic acid and 0.1% SDS) and digested as described in the figure legends. Digestion with Endo H was performed according to the supplier protocols. Digests were fractionated on 1.5-mm thick, 16.6% T/6% C Tricine SDS−PAGE gels (*26*, *27*). To identify radioactive fragments, a 5-mm wide vertical strip of the Coomassie blue stained gel was excised, cut into 2−5-mm slices, and counted, while the remainder of the gel was stored at 4 °C. The resulting ^{3}H profile was used as a template to identify the regions of the preparative gel containing ^{3}H. Material eluted from the gel was resuspended in the phosphate digestion buffer for digestion with V8 protease in solution or in that buffer supplemented with 1% Genapol C-100 (Calbiochem) for digestion with EndoAsp-N (2 μg, 25 °C, 7 days). After purification by SDS−PAGE, the eluted material (with or without additional protease treatment) was further purified by reversed-phase HPLC on a Brownlee Aquapore C-4 column (100 × 2.1 mm) at 40 °C. Solvent A was 0.09% trifluoroacetic acid in water, and solvent B was 60% acetonitrile/40% 2-propanol/0.05% trifluoroacetic acid. The gradients (in % solvent B) are indicated in the figures as dashed lines. The eluate (0.2 mL/min) was monitored by absorbance at 215 nm and by counting fraction aliquots (50 of 500 μL) for ^{3}H.

Sequence Analysis. Most N-terminal sequence analyses were performed on an Applied Biosystems Model 477A protein sequencer using gas-phase cycles optimized for sequencing on chemically modified glass-fiber peptide supports (Beckman #290111) (*28*). One-third of each cycle of Edman degradation was injected into an on-line Model 120A PTH-amino acid analyzer for residue identification and quantitation, and two-thirds were collected for ^{3}H counting. For the sequence analysis of the [^{3}H]TDBzcholine labeled material performed in the presence of α-BgTx (Figure 8), an Applied Biosystems Procise 492 sequencer was used with micro TFA filters (ABI # 401111), and one-sixth of each cycle was analyzed for amino acid identification and quantitation, while five-sixths were collected for ^{3}H counting. HPLC fractions of interest were drip-loaded directly onto the filters (45 °C) using a syringe pump. Residue amounts for PTH-amino acids were estimated from chromatographic peak heights. Values plotted are the actual cpm and background-subtracted pmol detected. The initial peptide amount (I_o) and the sequence run's repetitive yield (R) were calculated by nonlinear least-squares regression (Sigma Plot) of the function $f(n) = I_o \times R^n$ where $f(n)$ is the background subtracted pmol detected in cycle n. PTH-derivatives of Ser, Cys, Arg, His, and Trp were excluded from the fits. The specific ^{3}H incorporation into a labeled amino acid was determined by the equation $(cpm_n - cpm_{n-1})/(F \cdot pmol_n)$, where cpm_n is the ^{3}H detected in cycle n, $pmol_n$ is the calculated amount of the amino acid residue in cycle n, and F is 2 for sequencing on the 477A sequencer or 5 on the Procise 492 sequencer. In some cases, samples on the filter were treated with *o*-phthalaldehyde (Pierce) prior to cycles containing known proline residues. *o*-Phthalaldehyde reacts with primary, but not secondary, amines and will block Edman degradation of any peptide not containing an amino-terminal proline at the time of addition (*29*). *o*-Phthalaldehyde treatment was carried out as described (*22*).

Molecular Modeling. A model of the extracellular region of the *Torpedo* nAChR ($2\alpha_{(2-211)}$, $\beta_{(2-217)}$, $\gamma_{(2-219)}$, and $\delta_{(2-225)}$) was constructed from the high-resolution crystal structure of the snail acetylcholine binding protein (AChBP, ref *5*) as described previously (*30*). The structures of Bz_2-choline and TDBzcholine were constructed and minimized using the Builder module. These structures were placed within the ACh binding sites in multiple orientations to encourage unbiased sampling by the Docking module. A two subunit model was used for docking to simplify the computations, and the binding site was defined as α residues 93, 149, 150, 152, 188, 190, 192−194, 196, 198, and 200 and γ residues 55, 57, 59, 77, 109, 111, 117, and 119 (or the homologous residues in δ). For Bz_2choline docking at the α−γ agonist-site model, a total of 568 initial orientations within steric limitations were sampled, with a single orientation found 386 times upon minimization. For this favored orientation (Figure 9A), distances from the carbonyl oxygen were as follows: γLeu-109, 3.7 Å; γTyr-117, 3.1 Å; and αPro-194, 4.0 Å. TDBzcholine docking was performed at both the α−γ and α−δ agonist sites. For the α−γ site, when 633 orientations were sampled, 349 minimized to the orientation illustrated in Figure 9B. Distances to the photoreactive carbon of TDBzcholine were as follows: γLeu-109, 7.0 Å; γTyr-117, 4.6 Å; γGln-59, 3.8 Å; and αPro-194, 4.5 Å. For the α−δ agonist site, two equally favored orientations were obtained, one similar to the α−γ site orientation for TDBzcholine and the other differing by an ∼180° rotation of the diazirine so that it faces Segment C (not shown).

RESULTS

TDBzcholine Is a nAChR Antagonist. We examined the interactions of TDBzcholine with *Torpedo* nAChRs expressed in *Xenopus* oocytes. When applied alone at concentrations up to 100 μM, TDBzcholine elicited no detectable current response. When coapplied with 10 μM ACh, TDBzcholine produced a dose-dependent inhibition of ACh currents that was characterized by an IC_{50} of 0.3 μM and a Hill coefficient (n) of 1 (Figure 1A). Inhibition was completely reversible upon removal of TDBzcholine from the perfusion solution.

TDBzcholine Inhibition of the Binding of [^{3}H]ACh, [^{125}I]α-BgTx, and [^{3}H]HTX. In equilibrium binding studies with *Torpedo* nAChR-rich membranes, TDBzcholine fully inhibited the specific binding of 40 nM [^{3}H]ACh with an IC_{50} of 12 μM (n = 1.5) (●, Figure 1B). We also compared the TDBzcholine inhibition of the initial rate of binding of [^{125}I]α-BgTx with inhibition by the competitive antagonist D-tubocurarine (dTC, Figure 1C). Each drug reduced the rate of binding by >95% at high concentration, consistent with binding to the two ACh sites. For TDBzcholine, the concentration dependence of inhibition was well-fit by a single-site model with an IC_{50} of 14 μM, while, as expected (*31*), the dTC data were well-fit by a two-site model with K_D values of 30 nM and 4.5 μM (or by eq 1, IC_{50} = 0.3 μM and n = 0.4). TDBzcholine also inhibited the binding of the noncompetitive antagonist [^{3}H]HTX with an IC_{50} of 270 μM in the presence of carbamylcholine (Carb, Figure 1B) or dTC (not shown). These results establish that TDBzcholine binds to both ACh sites in the *Torpedo* nAChR as well as to an additional site probably within the ion channel but that

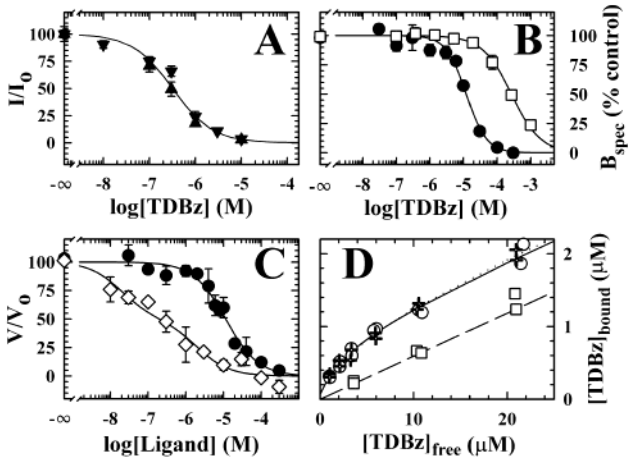

FIGURE 1: TDBzcholine is a *Torpedo* nAChR antagonist that binds to the two ACh sites with equal affinity. (A) TDBzcholine inhibition of ACh current responses for *Torpedo* nAChRs expressed in *Xenopus* oocytes. Currents (*I*) elicited by 3 μM ACh in the presence of TDBzcholine (from two separate syntheses (▲,▼)) were measured by a two-electrode voltage clamp and normalized to the currents (I_o) in the absence of TDBzcholine. The IC_{50} was 320 ± 20 nM (eq 1, single-site model). (B) TDBzcholine inhibition of the equilibrium binding of [3H]ACh (●, 30 nM) and [3H]HTX (□, 100 nM, in the presence of Carb) to *Torpedo* nAChR-rich membranes. The inhibition curves were fit to eq 1. For [3H]ACh, IC_{50} = 12 ± 1 μM and n = 1.5 ± 0.2; for [3H]HTX, IC_{50} = 265 ± 40 μM for a single-site model. (C) Inhibition of the initial rate of [125I]α-BgTx binding to nAChR-rich membranes by TDBzcholine (●) or dTC (◇). Rates of binding were determined in the absence (V_o) and presence (V) of inhibitor. The solid lines (—) represent the fit to eq 1 for TDBzcholine (IC_{50} = 14 ± 2 μM, n = 1) and the fit to eq 2 for dTC (K_H = 30 ± 18 nM and K_L = 4.5 ± 1.6 μM). (D) Equilibrium binding of [3H]TDBzcholine to nAChR-rich membranes was determined by centrifugation (−proadifen (+), +proadifen (○), or +proadifen/+Carb (□)). The calculated K_{eq} values were 1.9 ± 0.4 and 2.5 ± 0.8 μM in the absence and presence of proadifen.

TDBzcholine's affinity for the agonist sites is >20-fold higher than its affinity for the noncompetitive antagonist site.

Equilibrium Binding of [3H]TDBzcholine. The equilibrium binding of [3H]TDBzcholine to nAChR-rich membranes was measured (Figure 1D) in the absence or presence of proadifen, a desensitizing noncompetitive antagonist. [3H]-TDBzcholine binding in the presence of proadifen and Carb, which increased linearly with the free concentration, was used as a measure of the nonspecific binding. The specific binding of [3H]TDBzcholine was well-fit by a simple hyperbolic binding function characterized by K_{eq} = 3 μM in the absence or presence of proadifen, and the concentration of [3H]TDBzcholine binding sites (0.8 μM) was close to the concentration of [3H]ACh sites (1 μM).

Photoincorporation of [3H]TDBzcholine into nAChR-Rich Membranes. UV irradiation (360 nm) of nAChR-rich membranes equilibrated with 20 μM [3H]TDBzcholine resulted in covalent, agonist-inhibitable 3H incorporation into the α, γ, and δ subunits as determined by fluorography of a gel after SDS−PAGE fractionation of membrane polypeptides (Figure 2A, lanes 2 and 3). There was also agonist-inhibitable incorporation in a band with mobility close to that of rapsyn (43K protein) that is in a gel region known to contain a γ subunit degradation product (*24*). When the 3H incorporation into nAChR subunits was quantified by liquid scintillation counting of excised gel bands (Figure 2B), the agonist-

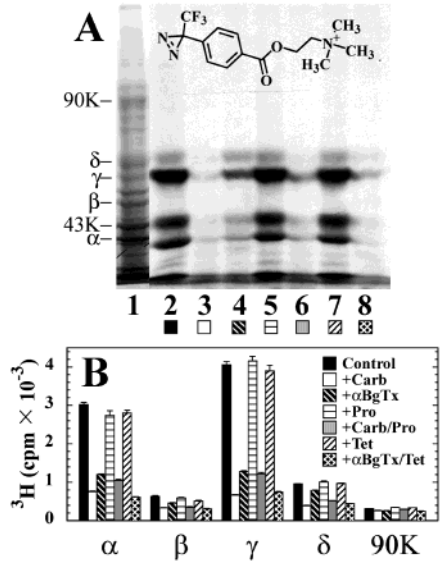

FIGURE 2: Effects of nAChR agonists and antagonists on the photoincorporation of [3H]TDBzcholine into nAChR-rich membranes. nAChR-rich membranes (60 μg, 90 pmol ACh sites in 100 μL of TPS) were equilibrated with 27 μM [3H]TDBzcholine either alone (lane 2), or with 1 mM Carb (lane 3), 10 μM α-BgTx (lane 4), 30 μM proadifen (lane 5), 1 mM Carb and 30 μM proadifen (lane 6), 30 μM tetracaine (lane 7), or 10 μM α-BgTx and 30 μM tetracaine (lane 8). Samples were irradiated for 30 min. (A) Polypeptides were resolved by SDS−PAGE, visualized by Coomassie Blue stain (lane 1), and processed for fluorography (lanes 2−8, 33-day exposure). Indicated on the left are the Coomassie-stained bands corresponding to the nAChR subunits, rapsyn (43K), and the α subunit of the Na/K ATPase (90K). (B) After fluorography, the visualized subunit bands were excised, and the 3H incorporation was determined by liquid scintillation counting.

inhibitable labeling within the γ subunit (3500 cpm) was highest, with labeling in the α and δ subunit bands at 66 and 15% that level. On the basis of the radiochemical specific activity of [3H]TDBzcholine, under the labeling conditions used, about 10% of the γ and 4% of the α subunits were labeled specifically.

As seen in the fluorogram, photolabeling of the nAChR subunits was not significantly altered by noncompetitive antagonists that bind preferentially in the ion channel either in the desensitized state (proadifen, ref *23*, lane 5) or the closed state (tetracaine, ref *32*, lane 7). However, subunit labeling was consistently lower in the presence of Carb (lane 3) than α-BgTx (lane 4), and for nAChRs photolabeled in the presence of α-BgTx and tetracaine (lane 8), the subunit labeling was reduced to the level in the presence of Carb. For the α and γ subunits, the tetracaine-inhibitable labeling seen in the presence of α-BgTx was about 20% of the level of agonist-inhibitable labeling, while for the δ subunit the tetracaine-inhibitable labeling was ~60% of the agonist-inhibitable labeling. These results indicated that in the absence of agonist [3H]TDBzcholine was specifically incorporated within the ACh sites, while the tetracaine-inhibitable subunit photolabeling seen in the presence of α-BgTx probably reflected [3H]TDBzcholine photoincorporation into a site within the ion channel.

Since [3H]TDBzcholine was bound with similar affinity to the two ACh sites but was photoincorporated into the nAChR γ subunit ~7-fold more efficiently than into the δ subunit, we wanted to determine whether the 3H incorporation within the α subunit reflected preferential photolabeling

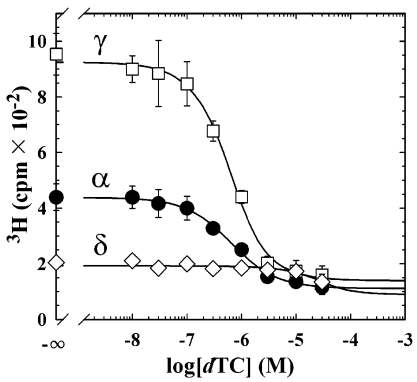

FIGURE 3: Concentration dependence of dTC inhibition of [^{3}H]-TDBzcholine photoincorporation into nAChR subunits. nAChR-rich membranes (300-μg aliquots, 370-pmol ACh sites) were equilibrated in 100 μL of TPS with 20 μM [^{3}H]TDBzcholine, 30 μM proadifen, and the indicated concentrations of dTC (10 nM to 30 μM) or 1 mM Carb. Each sample was then divided into three aliquots (30 μL) and irradiated for 30 min. After photolysis, the samples were fractionated by SDS−PAGE on three gels, and the gels were stained with Coomassie blue. Bands containing the nAChR α subunit (●), γ subunit (□), or δ subunit (◇) were excised, and ^{3}H incorporation was determined by scintillation counting. Shown are the averages with standard deviations for the three samples at each dTC concentration. When fit by eq 1 ($n = 1$), the dTC inhibition of the labeling of the α, γ, and δ subunits were characterized by IC_{50} values of 570 ± 70 nM, 590 ± 80 nM, and 25 ± 9 μM, respectively. The α subunit data were well-fit by a single-site model, with >90% of the specific (Carb inhibitable) labeling associated with the high affinity dTC binding site. Calculated K_i values for α, γ, and δ were 59 nM, 36 nM, and 26 μM, respectively. Nonspecific subunit photolabeling (+Carb): α, 106 ± 20 cpm; γ, 140 ± 35 cpm; and δ, 90 ± 2 cpm.

of one of the agonist sites, either at the α−γ subunit interface, where dTC binds with high affinity ($K_{eq} = 35$ nM), or at the site at the α−δ interface where dTC binds with low affinity ($K_{eq} \sim 4$ μM) (*31*). When nAChR-rich membranes were photolabeled with [^{3}H]TDBzcholine in the presence of various concentrations of dTC (Figure 3), dTC inhibition of the α subunit photolabeling was characterized by the same concentration dependence as for the γ subunit ($IC_{50} = 600$ nM, $n = 1$), while inhibition of the δ subunit photolabeling was seen only at dTC concentrations above 10 μM. Within the α subunit, the residual ^{3}H photolabeling seen in the presence of 10 μM dTC was the same as that seen in the presence of excess Carb. A dTC dissociation constant of 40−60 nM was calculated from the observed IC_{50} values in conjunction with the affinity and concentration of [^{3}H]-TDBzcholine and the concentration of nAChR used in the photolabeling study. Thus, >90% of the specific [^{3}H]-TDBzcholine photolabeling within the α subunit originated from the agonist site at the α−γ interface.

Identification of the Amino Acids Photolabeled by [^{3}H]-TDBzcholine in the α Subunit. We first mapped the sites of [^{3}H]TDBzcholine labeling within the four large nAChR α subunit fragments of 20, 18, 10, and 4 kDa that can be generated by in gel digestion with *S. aureus* V8 protease (designated αV8-20, αV8-18, αV8-10, and αV8-4, respectively, ref *24*). αV8-20 begins at αSer-173 and contains Segment C of the agonist binding site along with the M1, M2, and M3 hydrophobic segments. αV8-18 begins at αThr-52 and contains the agonist-site segments A and B as well as αAsn-142, the only site of Asn-linked glycosylation in the *Torpedo* α subunit. At least 90% of the agonist-

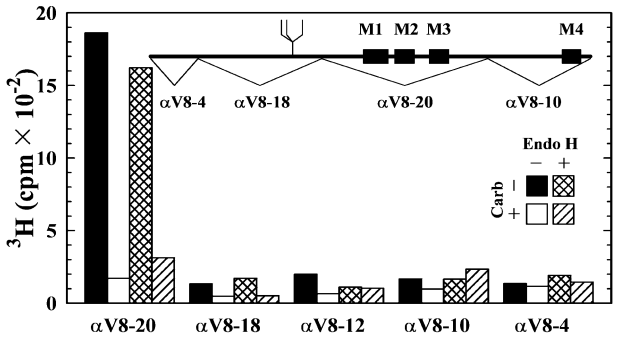

FIGURE 4: Mapping the site(s) of [^{3}H]TDBzcholine photoincorporation in the nAChR α subunit using *S. aureus* V8 protease. nAChR-rich membranes (18 mg, 18 nmol ACh binding sites in 4 mL) TPS were equilibrated with 35 μM [^{3}H]TDBzcholine and 40 μM proadifen in the absence or presence of 2 mM Carb. After 30 min irradiation, 600-μg aliquots were digested with 10 mU Endo H (0.5% SDS, 25 °C, 20 h) and then separated by SDS−PAGE along with equivalent amounts of nondeglycosylated samples. The α subunits were identified by Coomassie blue stain, excised, and transferred to a mapping gel for in gel V8 protease digestion and separation. The four characteristic α subunit fragments (αV8-4, αV8-18, αV8-20, and αV8-10, as in the schematic above) were visualized by Coomassie blue stain in the lanes containing glycosylated α subunit, whereas the 18-kDa fragment shifted to 12 kDa (αV8-12) upon Endo H treatment. The regions containing these bands were excised, and ^{3}H incorporation was determined by scintillation counting.

inhibitable photolabeling within the α subunit was contained within αV8-20 (Figure 4). This conclusion was confirmed by characterizing the distribution of ^{3}H when the deglycosylated α subunit was fragmented by V8 protease. Deglycosylation of αAsn-141 shifts the mobility of the fragment beginning at αThr-52 from 18 to 12 kDa, but it has no effect on the mobilities of the other fragments (*24*). Deglycosylation had no effect on the recovery of ^{3}H in αV8-20, and deglycosylation resulted in no redistribution of ^{3}H from 18 to 12 kDa. The amount of agonist-sensitive incorporation within the αV8-18 fragment, which contains the amino acids in ACh binding-site Segments A and B, was <5% of the specific incorporation in the α subunit.

To identify the residues in the α subunit labeled by [^{3}H]-TDBzcholine, the αV8-20 band was isolated by SDS−PAGE from nAChR-rich membranes photolabeled on a preparative scale (15 mg of protein) with [^{3}H]TDBzcholine in the absence and presence of Carb. When aliquots of αV8-20 were sequenced, there was a peak of ^{3}H release in cycles 20 and 21 for the sample labeled in the absence of agonist that was reduced by >90% for the sample labeled in the presence of agonist (Figure 5A). The primary sequence present began at αSer-173, and it was present at the same level in both samples ($I_o = 95$ pmol). Consistent with previous results (*25*), there were also secondary sequences beginning at αSer-162 (an alternative N-terminus of αV8-20, $I_o = 14$ pmol) and αV8-18 [αVal-46 ($I_o = 15$ pmol) and αThr-52 ($I_o = 6$ pmol)]. The observed ^{3}H release in cycles 20 (30 cpm) and 21 (60 cpm) would correspond to specific incorporation into αCys-192 and αCys-193 in the primary sequence at 1.8 and 4 cpm/pmol.

To confirm the identity of the residues photolabeled by [^{3}H]TDBzcholine, we characterized the ^{3}H incorporation in the fragments that could be isolated after labeled αV8-20 was digested with endoproteinase Lys-C (EndoLys-C), which is known to cleave αV8-20 after αLys-185 (*25*, *33*). When

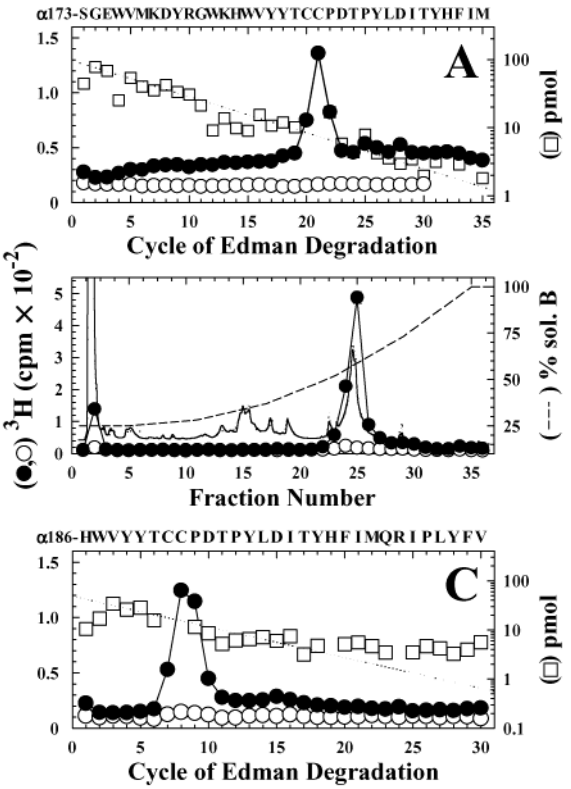

FIGURE 5: Identification of nAChR α subunit amino acids photolabeled by [^{3}H]TDBzcholine. nAChR-rich membranes (15 mg, 27 nmol ACh binding sites) were equilibrated with 20 μM [^{3}H]-TDBzcholine (●, −Carb; ○, +Carb) and irradiated, and then labeled αV8-20 (27 000 cpm −Carb; 1400 cpm +Carb) was isolated from a V8 protease mapping gel of α subunit. (A) ^{3}H and mass release upon sequencing αV8-20 for 35 cycles (●, 6750 cpm loaded, 3000 cpm left; ○, 340 cpm loaded, 170 cpm left). The primary sequence began at αSer-173 (□, −Carb, I_o = 96 pmol, R = 89%; +Carb, I_o = 93 pmol, R = 87%), with secondary sequences beginning at αVal-46 (15 pmol), αSer-162 (14 pmol), and αThr-52 (6 pmol). The ^{3}H release in cycles 20 and 21 would correspond to labeling of αCys-192 and αCys-193 in the primary sequence. (B) ^{3}H elution profile when aliquots of labeled αV8-20 were digested with EndoLys-C and the digests fractionated by reversed-phase HPLC, with 10% of each fraction assayed for ^{3}H (●, 18 900 cpm injected, 11 300 cpm recovered; ○, 950 cpm injected, 750 cpm recovered). Also shown are the absorption at 214 nm (—) and the % solvent B (- -). (C) ^{3}H and mass release when HPLC fractions 24 and 25 were pooled and sequenced for 30 cycles (●, 6000 cpm loaded, 1000 cpm left; ○, 160 cpm loaded, 40 cpm left). The primary sequence began at αHis-186 (□, −Carb, I_o = 48 pmol, R = 87%; +Carb, I_o = 49 pmol, R = 95%) with secondary sequences in both samples beginning at αAsp-180 (I_o = 7 pmol) and αSer-173 (I_o = 4 pmol). The ^{3}H release in cycles 7 and 8 corresponded to αCys-192 and αCys-193 from the primary sequence. After cycle 21 (in A) or cycle 8 (in C) in the −Carb samples, the sequencing filters were treated with *o*-phthalaldehyde to block Edman degradation of all peptides beginning with nonproline residues (*29*). The *o*-phthalaldehyde treatment corresponded to αPro-194 in the primary sequence from A (cycle 22) or C (cycle 9). Therefore, the subsequent release of ^{3}H in both samples corresponding to αPro-194 (A, cycle 22, 40 cpm; C, cycle 9, 90 cpm) cannot be attributed to a sequencing lag from the labeling at αCys-192 and αCys-193, and the observed ^{3}H release results from [^{3}H]TDBzcholine photolabeling of αPro-194. Levels of specific ^{3}H incorporation into αCys-192, αCys-193, and αPro-194 were 1.8, 4.0, and 3.0 cpm/pmol in A and 1.0, 2.3, and 3.3 cpm/pmol in B, respectively.

the digest was fractionated by reversed-phase HPLC, ∼80% of the recovered ^{3}H eluted in a single peak at ∼60% solvent B (Figure 5B), while undigested αV8-20 elutes at >90% solvent B (not shown). The two peak fractions were pooled for sequence analysis (Figure 5C). The primary sequence began at αHis-186 (−Carb, I_o = 48 pmol; +Carb, I_o = 49 pmol), and there were secondary sequences in both samples beginning at αAsp-180 (I_o = 7 pmol) and αSer-173 (I_o = 4 pmol). For the −Carb sample, there was release of ^{3}H in cycles 7 (35 cpm) and 8 (72 cpm) corresponding to αCys-192 and αCys-193 in the primary sequence, while no ^{3}H release was seen above background for the +Carb sample. The calculated specific incorporation at αCys-192 and αCys-193 was 1 and 2 cpm/pmol, respectively, which was similar to the specific incorporation calculated at those positions during the sequence analysis of αV8-20. During the sequencing of the −Carb sample, the filter had been treated with *o*-phthalaldehyde after cycle 8. *o*-Phthalaldehyde reacts with primary, but not secondary, amines and will block Edman degradation of any peptide without an amino-terminal proline at the time of addition (*29*), and the only sequence detected after cycle 8 was the primary sequence (with αPro-194 in cycle 9). The fact that the ^{3}H release in cycle 9 did not drop down to background, but remained at the same level as in cycle 8, indicates that the observed 90 cpm released in cycle 9 after *o*-phthalaldehyde treatment resulted from [^{3}H]-TDBzcholine labeling of αPro-194 at 3 cpm/pmol. In a control experiment (not shown), when a sample was treated with *o*-phthalaldehyde at a cycle immediately following a nonproline radiolabeled amino acid, the radioactivity released after treatment dropped to the background level. In the sequence analysis of αV8-20 (Figure 5A), where the sequencing filter had also been treated with *o*-phthalaldehyde after cycle 21, the ^{3}H release in cycle 22 (40 cpm) also indicates labeling of αPro-194 at 3 cpm/pmol.

[^{3}H]TDBzcholine Photoincorporation in the γ Subunit. Aliquots of the γ subunit isolated from nAChR-rich membranes photolabeled with [^{3}H]TDBzcholine were first characterized by digestion in gel with V8 protease. These studies established that the ^{3}H specifically incorporated in the γ subunit was contained within a single band of ^{3}H of ∼14 kDa and that for labeled γ subunit deglycosylated by Endo H, the band of ^{3}H had a mobility of ∼6 kDa (data not shown). These results indicated that the amino acid(s) photolabeled by [^{3}H]TDBzcholine were in a fragment produced by V8 protease that also contained γAsn-141, the only Endo H sensitive site of glycosylation in the *Torpedo* nAChR γ subunit (*9*). As work with the photoaffinity probes [^{3}H]dTC and [^{3}H]Bz$_2$choline had previously identified the amino-terminus of this peptide as γVal-102 (*9*, *10*), we utilized the strategies developed previously to identify the amino acids labeled by [^{3}H]TDBzcholine. Tricine SDS−PAGE was used to isolate the labeled fragment from an EndoLys-C digest of labeled γ subunit, which was then digested with V8 protease. The fragment beginning at γVal-102 was then isolated by reversed-phase HPLC.

Aliquots of labeled γ subunit (−Carb, 139 000 cpm; +Carb, 4400 cpm) were digested with EndoLys-C, and the digests were fractionated by preparative Tricine SDS−PAGE, with 10% of each digest placed in analytical lanes that were then cut into slices for liquid scintillation counting (Figure 6A). There was a single major peak of ^{3}H at ∼26 kDa. The corresponding Coomassie blue stained band (γEKC-26) was excised from the preparative Tricine gel and eluted. Sequence analysis of an aliquot of labeled γEKC-26 identified subunit

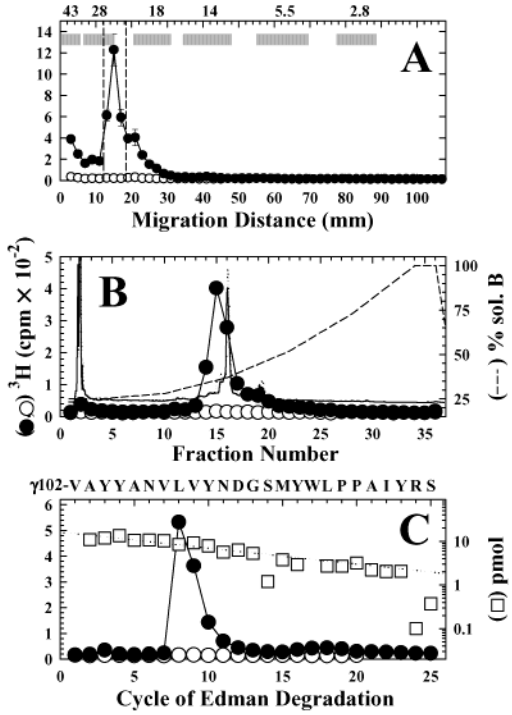

FIGURE 6: [^{3}H]TDBzcholine photolabels γ subunit residue Leu-109. nAChR-rich membranes (15 mg, 27 nmol ACh-binding sites) were equilibrated with 20 μM [^{3}H]TDBzcholine (●, −Carb; ○, +Carb) and irradiated, and the labeled γ subunit was isolated by SDS−PAGE. The labeled γ subunit (●, 138 600 cpm, 1000 cpm/μg; ○, 4400 cpm, 20 cpm/μg) was digested with EndoLys-C (1.5 U each, 3 weeks, 25 °C), and the resulting fragments were separated by Tricine SDS−PAGE. (A) The distributions of ^{3}H from lanes of the Tricine gel containing 10% of each digest, as determined by gel slice analysis (2-mm slices). The mobilities of the prestained molecular mass markers are indicated above. The band of ^{3}H at ∼26 kDa (γEKC-26) (with an associated Coomassie blue stained band) was excised from the remainder of the gels, eluted, and concentrated. Sequence analysis of γEKC-26 (10%) from the −Carb sample revealed γ subunit fragments beginning at γArg-18 (I_o = 3.2 pmol, R = 91%), γThr-24 (I_o = 2.2 pmol, R = 93%), and γGlu-47 (I_o = 1.3 pmol, R = 95%). (B) ^{3}H elution profile when the γEKC-26 samples were digested with V8 protease in solution and the digests fractionated by reversed-phase HPLC, with 10% of each fraction assayed for ^{3}H (●, 13 260 cpm injected, 13 130 cpm recovered; ○, 225 cpm injected, 360 cpm recovered). Also shown are the absorption at 214 nm (—) and the % solvent B (- -). (C) ^{3}H and mass release when HPLC fraction 15 was sequenced for 25 cycles (●, 3500 cpm loaded, 500 cpm left; ○, 5 cpm loaded). The primary sequence began at γVal-102 (□, −Carb, I_o = 16 pmol, R = 92%; +Carb, I_o = 25 pmol, R = 91%). The only additional sequence detected (>1 pmol) began at the amino terminus of V8 protease (I_o = 5 pmol). The ^{3}H release in cycle 8 (508 cpm) was consistent with [^{3}H]TDBzcholine incorporation into γLeu-109 at 31 cpm/pmol.

fragments beginning at γArg-18 (I_o = 3 pmol), γThr-24 (I_o = 2 pmol), and γGlu-47 (I_o = 1 pmol). No release of ^{3}H more than 1 cpm above background was detected through 22 cycles of Edman degradation, which included in cycle 9 the primary site of [^{3}H]dTC photoincorporation in the γ subunit, γTrp-55 (0.8 pmol) (*25*). γEKC-26 was digested with V8 protease, and the digest was fractionated by reversed-phase HPLC (Figure 6B). There was a single peak of ^{3}H that eluted at ∼37% solvent B and contained ∼70% of the recovered ^{3}H. When the peak fraction was sequenced, there was specific release of ^{3}H in cycle 8, and the only γ subunit peptide present began at γVal-102 (−Carb, I_o = 16 pmol; +Carb, I_o = 25 pmol, Figure 6C). The only other peptide present at more than 1 pmol began at Val-1 of V8 protease (5 pmol). The ^{3}H release in cycle 8 (508 cpm) corresponded to [^{3}H]TDBzcholine incorporation into γLeu-109 at a specific activity of 30 cpm/pmol.

[^{3}H]TDBzcholine Photoincorporation in the δ Subunit. Although [^{3}H]TDBzcholine was photoincorporated into the δ subunit at only ∼15% the efficiency of the γ subunit, we wanted to determine whether that incorporation was in δLeu-111, the position in the δ subunit equivalent to γLeu-109, or in nearby amino acids. To accomplish this, we used the digestion and purification strategies developed in studies of [^{3}H]Bz$_2$choline to isolate a fragment beginning at δAsp-99 (*10*). Aliquots of the labeled δ subunit (−Carb, 33 400 cpm; +Carb, 4200 cpm) were first digested with EndoLys-C and separated by preparative Tricine SDS−PAGE, with 10% of each digest in separate analytical lanes for analysis of ^{3}H distribution by scintillation counting (Figure 7A). In the analytical lane, the ^{3}H was in a band of ∼21 kDa (δEKC-21), and in the preparative gel there was a band in this region stained by Coomassie blue that was excised and eluted (−Carb, 6800 cpm; +Carb, 270 cpm). Sequence analysis of 10% of this material revealed fragments beginning at δHis-20 (I_o = 7 pmol) and δHis-26 (I_o = 7 pmol). No release of ^{3}H more than 2 cpm above background was seen during 15 cycles of Edman degradation.

Aliquots of the 21-kDa band (−Carb, 6000 cpm; +Carb, 225 cpm) were then digested with EndoAsp-N, and the digests were fractionated by reversed-phase HPLC (Figure 7B). The ^{3}H was recovered in two peaks, centered at 35 and 42% solvent B (fractions 16 and 19). Sequence analysis of fraction 16 (Figure 7C) revealed the presence of the peptide beginning at δAsp-99 (I_o = 23 pmol), as well as fragments beginning at δAsp-76 (49 pmol), δHis-26 (14 pmol), and δHis-20 (12 pmol). The prominent release of ^{3}H seen in cycle 13 (90 cpm) (Figure 7C) would correspond to incorporation at δLeu-111. This ^{3}H release appeared specific since no release was seen for the +Carb sample. However, the mass recoveries for the +Carb sample were only 10−20% that for the −Carb sample, so further experimentation will be required to prove the specificity of this labeling. When fractions 17, 18, and 19 were individually sequenced, all three also contained the peptide beginning at δAsp-99 with ^{3}H release in cycle 13 at 10−20 cpm (Figure 7D). To determine whether the ^{3}H release in cycle 13 correlated with the amount of δLeu-111, we calculated the cpm released/pmol δLeu-111 from the initial and repetitive yields of the δAsp-99 fragment in each fraction. For each fraction, the ^{3}H release in cycle 13 was consistent with labeling of δLeu-111 at 4−5 cpm/pmol. In contrast, the ^{3}H release in cycle 13 of each fraction did not correlate well with the amount of the δAsp-76 fragment, varying from 2 to 60 cpm/pmol, and sequence analysis of δEKC-21 beginning at δHis-20/26 had no ^{3}H release. During sequence analysis of fraction 16 (Figure 7C), ^{3}H release was also seen in cycle 4 at low level (20 cpm), while for fractions 17−19, the ^{3}H release in cycle 4 was <3 cpm. The amount of ^{3}H release in cycle 4 did not correlate well with the amount of the δAsp-99 fragment in each fraction, and further work will be required to determine whether there is an amino acid in addition to δLeu-111 that is labeled by [^{3}H]TDBzcholine.

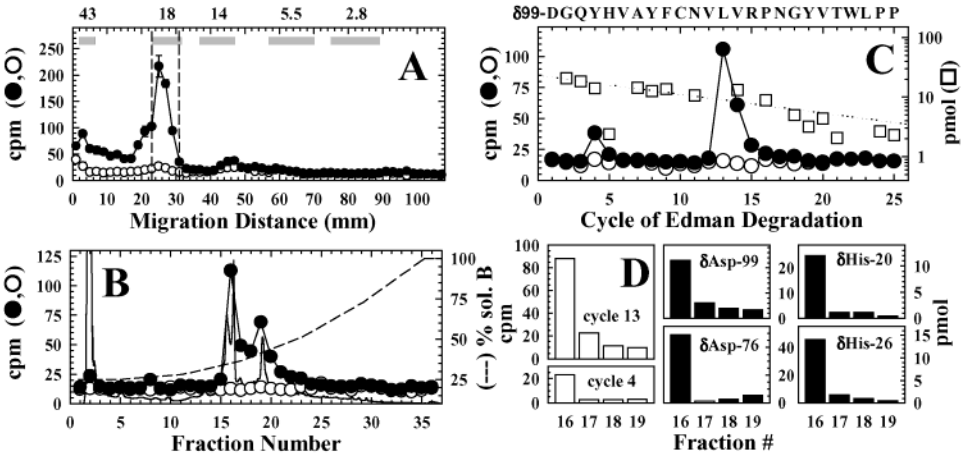

FIGURE 7: [3H]TDBzcholine photolabels δ subunit residue Leu-111. [3H]TDBzcholine labeled δ subunit (−Carb (●), 33 400 cpm; +Carb (○), 4200 cpm) from the labeling described in Figure 6 was digested with EndoLys-C (1.5 U each, 3 weeks, 25 °C), and the resulting fragments were separated by Tricine SDS−PAGE. (A) 3H distribution from an analytical lane of the Tricine gel (10% of each digest) determined by gel slice analysis (2-mm slices). The mobilities of the prestained molecular mass markers are indicated above. The band of 3H at ∼21 kDa (δEKC-21) was associated with a Coomassie blue stained band that was excised from the remainder of the gels, eluted, and concentrated. Sequence analysis of 10% of the δEKC-21 (−Carb) indicated the presence of δ subunit fragments beginning at δHis-20 (I_o = 7 pmol, R = 94%) and δHis-26 (I_o = 7 pmol, R = 88%). (B) 3H elution profile when the δEKC-21 samples were digested with EndoAsp-N in solution and the digests fractionated by reversed-phase HPLC, with 10% of each fraction assayed for 3H (●, 5960 cpm injected, 4420 cpm recovered; ○, 225 cpm injected, 275 cpm recovered). Also shown are the absorption at 214 nm (—) and the % solvent B (- -). 62% of the recovered 3H eluted in a double peak between fractions 16 and 19. (C) 3H and mass release when HPLC fraction 16 was sequenced for 25 cycles (●, 910 cpm loaded, 250 cpm left; ○, 5 cpm loaded). δ subunit fragments were identified beginning at δAsp-99 (□, −Carb, I_o = 23 pmol, R = 93%; +Carb, I_o = 2 pmol, R = 89%), δAsp-76 (−Carb, I_o = 49; +Carb, I_o = 6), δHis-26 (−Carb, I_o = 14; +Carb, I_o = 4), and δHis-20 (−Carb, I_o = 12; +Carb, I_o = 2). (D) Results from the sequence analyses of fractions 16−19 (−Carb) from the HPLC in B. Plotted are the 3H released in sequencing cycles 13 and 4 as well as the initial amounts (I_o in pmol) of the δ subunit fragments. I_o values for the fragment beginning at δAsp-99: fraction 17, 6 pmol; fraction 18, 4 pmol; and fraction 19, 3 pmol. The calculated incorporation of 3H at δLeu-111 (cycle 13) for fractions 16−19 was 5.0, 5.4, 4.4, and 5.5 cpm/pmol, respectively.

[3H]TDBzcholine Photoincorporation in the Ion Channel. When nAChRs were photolabeled with[3H]TDBzcholine in the presence of α-BgTx, there was 3H photoincorporation into each nAChR subunit that was inhibitable by tetracaine (Figure 2), which binds with high affinity to a site in the ion channel (*32*, *34*). To begin to identify the site(s) of labeling, the δ subunits were isolated by SDS−PAGE from 15-mg aliquots of nAChR-rich membranes photolabeled with [3H]TDBzcholine (35 μM) after equilibration with α-BgTx in the absence or presence of tetracaine. To determine whether there was photolabeling within the δ subunit M2 hydrophobic segment, the δ subunits were digested with EndoLys-C, which cleaves after δLys-256 to produce an ∼10 kDa fragment beginning at δMet-257, the N-terminus of δM2 (*34*). When the digest was fractionated by reversed-phase HPLC, there was a single peak of 3H centered at ∼60% solvent B (Figure 8A). Sequence analysis of the peak 3H fraction revealed release of 3H in cycle 13 that was reduced by >90% for the sample labeled in the presence of tetracaine (Figure 8B). This fraction contained the peptide beginning at δMet-257 (− or + tetracaine, I_o = 20 pmol) as well as fragments beginning at δPhe-206 (18 pmol) and δAsn-437 (17 pmol)[2] that contain the δM1 and δM4 hydrophobic segments, respectively. Since a two-step purification using SDS−PAGE and reversed-phase HPLC had been required to isolate in high purity the fragment beginning at δMet-257 (*34*), we did not expect to be able to separate that fragment from the other hydrophobic fragments by reversed-phase HPLC alone. However, the 3H release in cycle 13 would correspond to labeling of δVal-269 (−tetracaine, 13 cpm/pmol; +tetracaine, 0.7 cpm/pmol,) within δM2, an amino acid previously shown to contribute to the binding site for 3-(trifluoromethyl)-3-(*m*-[125I]iodophenyl)diazirine-([125I]TID) and [3H]tetracaine in the nAChR ion channel in the closed state (*34*, *35*).

DISCUSSION

In this report we introduce TDBzcholine as a photoreactive nAChR antagonist and identify the amino acids in the ACh binding sites that it photolabels. TDBzcholine contains a photoreactive diazirine at the para-position of benzoylcholine (i.e., 10 Å from the quaternary ammonium and in the same position as the photoreactive ketone in Bz_2choline). However, for TDBzcholine the substituent is smaller in size than the benzoyl substitution of Bz_2choline, and the mechanism of reactivity of its carbene intermediate differs significantly from that of the ketyl radical formed upon excitation of benzophenones. Carbenes react preferentially with different side chains than benzophenones, and in addition, they react very efficiently with water (*18*, *36*).

[3H]Bz_2choline bound with equal affinity to the two ACh sites and photoincorporated selectively into a single amino acid in each ACh binding site: γLeu-109 and δLeu-111, amino acids that occupy equivalent positions in ACh binding-site Segment E (*10*). It was surprising to find a nAChR

[2] There was also a fragment beginning at δAsn-447 (9 pmol) that would result from a cleavage after δTrp-446. Such a fragmentation was unexpected after digestion with EndoLys-C, and in control experiments we determined that it actually occurred when the sample was applied to the sequencing filter. When peptides in HPLC solvent containing 0.05% TFA are applied to Biobrene treated glass fiber filters (ABI #401111) heated to 45 °C, we have found reproducibly cleavage on the N-terminal side of Trp residues (data not shown).

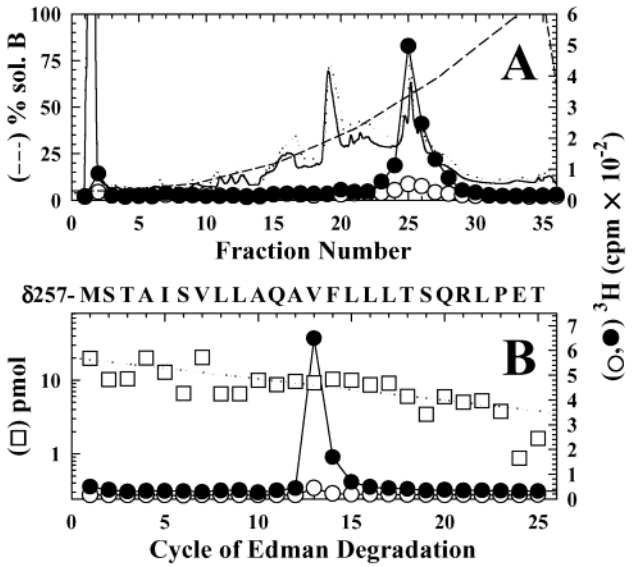

FIGURE 8: [^{3}H]TDBzcholine photoincorporation in the ion channel. nAChR-rich membranes (15 mg, 27 nmol ACh-binding sites) were preincubated with 100 nmol α-BgTx for 1 h, then equilibrated with 20 μM [^{3}H]TDBzcholine in the absence (●) or presence (○) of 10 μM tetracaine, and irradiated. After photolysis, labeled δ subunit (●, 19 200 cpm (40 cpm/μg); ○, 3520 cpm (11 cpm/μg)) was isolated by SDS−PAGE and then digested with EndoLys-C (1.5 U each, 3 weeks, 25 °C). The digests were fractionated by reversed-phase HPLC. (A) ^{3}H elution profile, with 10% of each fraction assayed for ^{3}H (●, 17 300 cpm injected, 13 200 cpm recovered; ○, 3170 cpm injected, 2500 cpm recovered). Also shown are the absorption at 214 nm (—) and the % solvent B (- -). (B) ^{3}H and mass release when HPLC fraction 25 was sequenced for 30 cycles (●, 4400 cpm loaded, 420 cpm left; ○, 360 cpm loaded). δ subunit fragments were identified beginning at δMet-257 (□, I_o = 21 pmol, R = 94%) as well as δPhe-206 (I_o = 18 pmol, R = 94%) and δAsn-447 (I_o = 9 pmol, R = 93%), each at the same mass levels for the two samples. ^{3}H release in cycle 13 (●, 606 cpm; ○, 30 cpm) was consistent with tetracaine-inhibitable [^{3}H]TDBzcholine incorporation into δVal-269 (12 cpm/pmol) in the M2-hydrophobic segment.

photoaffinity competitive antagonist that incorporated with such selectivity into binding-site amino acids in the γ and δ subunits without reacting with α subunit amino acids, especially since benzophenones can have broad side-chain reactivity (*18*, *37*). As we discuss later, this selective reactivity remains surprising in view of the structure of the ACh binding site in the AChBP (*5*).

Although benzoylcholine itself is a low efficacy partial agonist for *Torpedo* nAChRs expressed in *Xenopus* oocytes (unpublished observations), we found that TDBzcholine did not activate nAChRs, and it was a potent inhibitor (IC_{50} = 0.3 μM) of ACh responses. On the basis of the inhibition of binding of [^{3}H]ACh (IC_{50} = 12 μM) or [^{125}I]α-Bgtx (IC_{50} = 14 μM) to *Torpedo* nAChR-rich membranes, TDBzcholine binds with equal affinity to the two agonist sites, while the inhibition of binding of [^{3}H]HTX (IC_{50} = 260 μM) indicates that TDBzcholine interacts >20-fold more weakly with the ion channel. In view of the observed affinities of TDBzcholine for the ACh and noncompetitive antagonist binding sites, the submicromolar potency seen for the inhibition of *Torpedo* nAChRs expressed in oocytes was surprising. However, this difference was seen for two independent syntheses of TDBzcholine that were each used in parallel binding and electrophysiological studies, and it likely reflects differences between the nAChRs in oocytes and in electric organ membranes.

Analysis of the pattern of [^{3}H]TDBzcholine photoincorporation at the level of nAChR subunits revealed agonist-inhibitable photolabeling into the α subunit as well as in the γ and δ subunits. On the basis of the ^{3}H incorporation in the bands containing the nAChR subunits, for the labeling conditions used, ~10% of the γ, 4% of the α, and 2% of the δ subunits were specifically labeled. The reduced labeling of the δ subunit as compared to the γ subunit did not occur because of preferential photoincorporation into binding-site amino acids within the α subunit of the α−δ site. On the basis of the concentration dependence of the dTC inhibition of labeling (Figure 3), >90% of α subunit labeling was within the α subunit contributing to the high affinity dTC site (i.e., the binding site at the α−γ interface, ref *31*). The inefficient labeling of amino acids within the α−δ binding site also differs from the pattern of photolabeling seen for the agonist [^{3}H]nicotine that was photoincorporated into the γ subunit at >10-fold higher efficiency than the δ subunit but into the two α subunits with similar efficiency (*22*).

Agonist Binding-Site Amino Acids Photolabeled by [^{3}H]-TDBzcholine. [^{3}H]TDBzcholine was photoincorporated with highest efficiency into the nAChR γ subunit, and we identified the primary amino acid labeled as γLeu-109 in binding-site Segment E, the same amino acid labeled by [^{3}H]Bz$_2$choline (*10*). The level of ^{3}H incorporation in γLeu-109 (30 cpm/pmol) indicated that ~6% of subunits were labeled at that position. The efficient labeling of γLeu-109 and the residual release of ^{3}H from that amino acid in subsequent cycles of Edman degradation (Figure 6C) would obscure ^{3}H incorporation in γTyr-111, which was labeled by [^{3}H]dTC (*9*), unless it was labeled at >20% the level of labeling of γLeu-109. γTyr-117, which was also photolabeled by [^{3}H]dTC, is paired with γLeu-109 in the antiparallel β-strands the make up Segment E (Figure 9). The observed ^{3}H release profile seen during sequence analysis of the fragment beginning at γVal-102 indicated that any labeling of γTyr-117 or of γLeu-119 was at <4% the level of incorporation into γLeu-109. In addition, sequence analysis of the EndoLys-C γ subunit fragment beginning at γGlu-46 established that if [^{3}H]TDBzcholine photolabeled γTrp-55 or adjacent amino acids, it was at <5% the level of labeling of γLeu-109. Thus, the orientation of the reactive carbene in the binding site is defined by the selective labeling of γLeu-109.

[^{3}H]TDBzcholine photolabeling of the δ subunit was at ~15% the efficiency of the γ subunit. Because of this inefficient labeling, we first examined whether there was labeling of δLeu-111, the residue homologous to γLeu-109. Although the fragment beginning at δAsp-99 was not completely purified, there was a good correlation between the amount of that fragment in sequential HPLC fractions and the level of ^{3}H release seen in cycle 13, the cycle containing δLeu-111, and there was a poor correlation with the level of the fragment beginning at δAsp-76. The level of ^{3}H incorporation in δLeu-111 (5 cpm/pmol) indicated that only ~1% of δ subunits were labeled at that position but that this amino acid is the major site of incorporation in the δ subunit.

[^{3}H]TDBzcholine photolabeling was restricted to the α subunit present at the interface with the γ subunit that makes

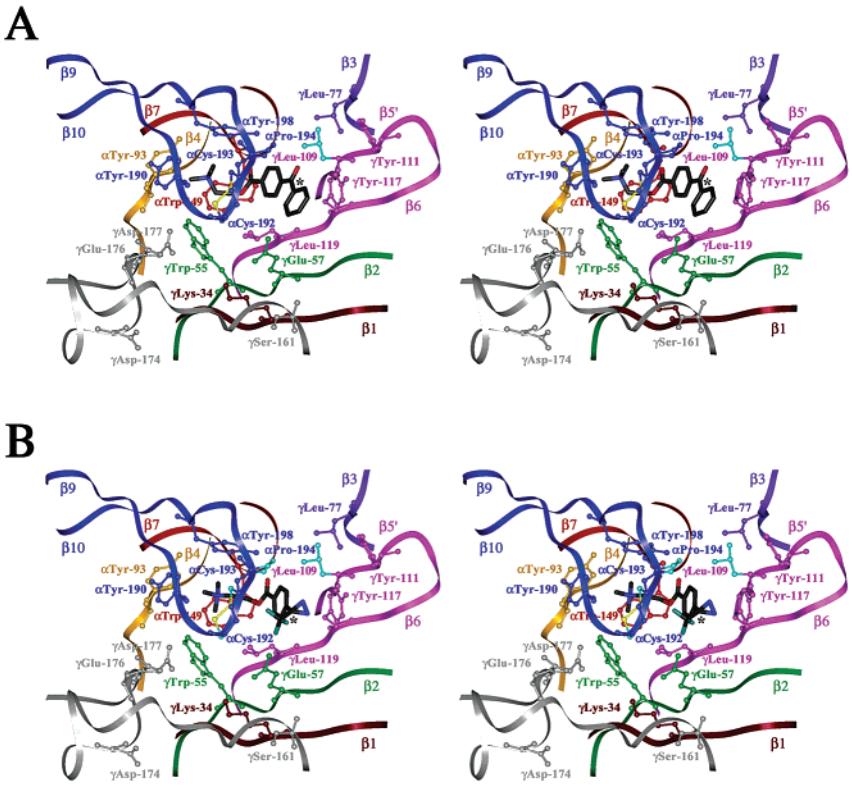

FIGURE 9: Stereo representation of Bz_2choline and TDBzcholine within the *Torpedo* nAChR α-γ agonist binding site. A homology model of the nAChR was constructed from the crystal structure of the AChBP (*5*), and Bz_2choline (A) or TDBzcholine (B) were docked within the identified ACh binding site located at the interface between an α and the γ subunits. Shown in ribbon representation are the segments of primary structure located near the agonist site. β-sheets identified for the AChBP structure are denoted (β1, β2, ...). The ligands are shown in stick representation with their atoms color coded: carbon, black; nitrogen, blue; oxygen, red; and fluorine, turquoise. Hydrogens were omitted for simplification. Selective amino acids residues are denoted in ball-and-stick representation with different colors representing different segments of the primary structure localized near the agonist binding site: Segment A (α93), gold; Segment B (α149), red; Segment C (α190−198), blue (with the sulfurs of αCys-192/192 in yellow); Segment D (γ55−57), green; Segment E (γ109−119), magenta; and Segment F (γ174), silver. Also included are segments containing γ34 (brown) and γ77 (purple). The photoreactive carbons for the two ligands are denoted by the asterisks, and the residues labeled by the respective compounds are cyan.

up the high affinity dTC binding site, and within that α subunit >90% of agonist-inhibitable labeling was in a 20-kDa fragment that contained amino acids of agonist binding-site Segment C (α190−198). [3H]TDBzcholine did not photolabel αTyr-190 or αTyr-198, binding-site amino acids photolabeled by [3H]dTC (*25*) and [3H]nicotine (*22*), but it did photoincorporate into αCys-192 and αCys-193 at 2 and 4 cpm/pmol, respectively. In addition, we provide evidence that αPro-194, which has not been previously identified as a binding-site amino acid by affinity labeling, is specifically photolabeled by [3H]TDBzcholine. With 3H incorporation in αCys-192/193, proof that αPro-194 was also labeled depended upon the use of *o*-phthalaldehyde at the sequencing cycle containing αPro-194. For example, in the sequence analysis of the fragment beginning at αHis-186 (Figure 5C), there was no increase in 3H release from cycle 8 (αCys-193) to 9 (αPro-194), but the 3H release in cycle 9 is associated with αPro-194 since the only amino acid released by Edman degradation at that cycle after treatment with *o*-phthalaldehyde was αPro-194. The calculated level of labeling of αPro-194 (3 cpm/pmol) was similar when fragments were sequenced beginning at αSer-173 (Figure 5A) and αHis-186 (Figure 5C), and the level of labeling was the same as the incorporation into αCys-192 or αCys-193.

[3H]TDBzcholine Photolabels the Ion Channel in the Resting State. In addition to the agonist-inhibitable labeling of amino acids within the agonist binding sites, for nAChRs photolabeled by [3H]TDBzcholine in the presence of α-BgTx, there was tetracaine inhibitable labeling into the α, γ, and δ subunits that was seen both by fluorography and by gel slice analysis (Figure 2). We carried out preliminary experiments with the labeled δ subunit that indicated a pattern of 3H release during sequence analysis consistent with the labeling of δVal-269, the 13th amino acid in the M2 hydrophobic segment and one of the amino acids photolabeled in the nAChR ion channel in the closed state by [125I]TID and [3H]-tetracaine (*34*, *35*). Because only a one-step purification of a labeled fragment from an EndoLys-C digest of δ subunit was used before sequence analysis, further studies would be required to prove that the observed release originates from δVal-269 and not from the other fragments also present that began at δPhe-206 and δAsn-437, 19 and 22 amino acids before the beginning of δM1 and δM4, respectively. However, as the labeling of δVal-269 is consistent with conclusions concerning the structure of the noncompetitive antagonist site in the closed channel, we feel there is little doubt that this is the labeled amino acid. The level of labeling (12 cpm/pmol) indicates that about 4% of δ subunits were labeled. Since the IC_{50} for TDBzcholine inhibition of [3H]-HTX binding was 0.3 mM, this suggests that under the conditions of photolabeling (20 μM [3H]TDBzcholine), site occupancy was less than 10%, which suggests that the efficiency of photolabeling was in fact very high.

TDBzcholine, Bz_2choline, and a Homology Model of the nAChR Agonist Site. When Bz_2choline and TDBzcholine are docked in the ACh binding site at the $\alpha-\gamma$ interface in a homology model of the nAChR based upon the structure of the AChBP (Figure 9), for each ligand the quaternary ammonium occupies the binding pocket made up by the aromatic side chains from αTyr-93, αTrp-149, αTyr-190, αTyr-198, and γTrp-55, and the substituted benzoic acid is oriented toward amino acids in Segment E (β5′ and β6) and Segment D (β2). In the homology model, γLeu-109/δLeu-111 is the closest side chain in Segment E to αPro-194, at a distance of 6 Å. For Bz_2choline (Figure 9A), the ketone oxygen is closest to γLeu-109 and αPro-194, with the carbonyl carbon within 5 Å of γLeu-109 and γGln-59 and 4 Å of γTyr-117 and αPro-194. While the labeling of γLeu-109/δLeu-111 is consistent with the model, the selectivity of labeling is not predicted. Factors that could account for the observed selective labeling include: (i) the proximity relations in the model of the binding site could be generally appropriate, with the selective labeling resulting from preferential reactivity with the Leu side chain rather than Pro or Tyr, or (ii) the distance between αPro-194 and δLeu-109 in the nAChR binding site in the conformation labeled by [^{3}H]Bz_2choline may be significantly greater than the distance in the homology model. Comparison of the 4.6 Å cryoelectronmicroscopy structure of the *Torpedo* nAChR with that of the AChBP indicates that, in the nAChR resting state, binding-site Segment C is less closely associated with the surface of the γ or δ subunit (*11*).

In contrast with the selective labeling of γLeu-109/δLeu-111 by [^{3}H]Bz_2choline, the [^{3}H]TDBzcholine photolabeling results predict that αPro-194 is in close proximity to γLeu-109 (as well as to the reactive carbene at the para-position of benzoylcholine), consistent with the predicted structure of the binding site in the homology model. When docked in the binding site at the $\alpha-\gamma$ interface in the homology model (Figure 9B), TDBzcholine adopts an orientation shifted subtly relative to that of Bz_2choline, and the photoreactive carbon is within 5 Å of αPro-194, γGlu-57, and γTyr-117 and within 7 Å of αCys-193 and γLeu-109. Since the reactive carbene formed by TDBzcholine reacts, at least in a model system, with ∼10-fold higher efficiency with Cys or Trp than with Pro or Leu (*36*), the preferential labeling of γLeu-109 (30 cpm/pmol) as well as the labeling of αPro-194 at similar levels as αCys-193 (2−4 cpm/pmol) argues strongly that in the nAChR agonist binding site, the carbene is closest to γLeu-109 and αPro-194. The orientation of TDBzcholine in the binding site is further constrained by the fact that it reacts with γLeu-109 at >25-fold higher efficiency than either γLeu-119, which will have the same intrinsic side-chain reactivity as γLeu-109 or γTyr-117. (The same carbene in [^{125}I]TID reacts readily with Tyr and many other aromatic and aliphatic side chains in the nAChR transmembrane domain, refs *35*, *38*.)

The specific photolabeling of δLeu-111 indicates that TDBzcholine binds in the $\alpha-\delta$ site in a similar orientation as in the $\alpha-\gamma$ site. As seen for Bz_2choline, TDBzcholine binds with similar affinities in the two sites, but in contrast to [^{3}H]Bz_2choline, which labeled γLeu-109 and δLeu-111 with similar efficiencies, [^{3}H]TDBzcholine labeled δLeu-111 at only 15% that of γLeu-109 and that reduced labeling was not compensated by the labeling of other amino acids in the α or δ subunit. In the homology model of the nAChR, the general structure of the $\alpha-\delta$ site is similar to that of the $\alpha-\gamma$ site, with δLeu-111 6.3 Å from αPro-194. When docked in that site, TDBzcholine adopts an orientation similar to that in the $\alpha-\gamma$ site with the photoreactive carbon within 5 Å of δAsp-59 and δThr-119 and 7 Å of αCys-193, αPro-194, δLeu-111, and δLeu-121 (not shown). The model does not explain the inefficient labeling at the $\alpha-\delta$ site, and the photolabeling results suggest that there are structural differences between the sites that are not predicted by the model. One possibility is that the distance between δLeu-111 and αPro-194 is greater than that between γLeu-109 and αPro-194 (i.e., the $\alpha-\delta$ site has a more relaxed structure). Another possibility is that the general backbone structures are similar, but the unique side chains contributed from the γ and δ subunits create distinct local environments. In the *Torpedo* nAChR, γTyr-111 is replaced by δArg-113, and γTyr-117 is replaced by δThr-119. One notable difference between the photoreactive intermediates formed by Bz_2choline and TDBzcholine is the fact that the ketyl diradical of the former cannot react with water, while the carbene of TDBzcholine reacts very efficiently with water. It is possible that the additional aromatic side chains within the $\alpha-\gamma$ site contribute to a more hydrophobic binding pocket where water is excluded. While studies with Bz_2choline and TDBzcholine define the binding-site orientation of two antagonists, in the future it will be important to map the orientation of aromatic choline esters that act as agonists to determine, for example, whether they are oriented toward amino acids on β6 (γTyr-117/Leu-119).

REFERENCES

1. Corringer, P.-J., Le Novere, N., and Changeux, J.-P. (2000) *Annu. Rev. Pharmacol. Toxicol. 40*, 431−458.
2. Arias, H. R. (2000) *Neurochem. Int. 36*, 595−645.
3. Karlin, A. (2002) *Nat. Rev. Neurosci. 3*, 102−114.
4. Smit, A. B., Syed, N. I., Schaap, D., van Minnen, J., Klumperman, J., Kits, K. S., Lodder, H., van der Schors, R. C., van Elk, R., Sorgedrager, B., Brejc, K., Sixma, T. K., and Geraerts, W. P. M. (2001) *Nature 411*, 261−268.
5. Brejc, K., van Dijk, W. J., Klaassen, R., Schuurmans, M., van der Oost, J., Smit, A. B., and Sixma, T. K. (2001) *Nature 411*, 269−276.
6. Sine, S. M. (1993) *Proc. Natl. Acad. Sci. U.S.A. 90*, 9436−9440.
7. Sine, S. M., Kreienkamp, H. J., Bren, N., Maeda, R., and Taylor, P. (1995) *Neuron 15*, 205−211.
8. Sine, S. M. (1997) *J. Biol. Chem. 272*, 23521−23527.
9. Chiara, D. C., Xie, Y., and Cohen, J. B. (1999) *Biochemistry 38*, 6689−6698.
10. Wang, D., Chiara, D. C., Xie, Y., and Cohen, J. B. (2000) *J. Biol. Chem. 275*, 28666−28674.
11. Unwin, N., Miyazawa, A., Li, J., and Fujiyoshi, Y. (2002) *J. Mol. Biol. 319*, 1165−1176.
12. Silman, I., and Karlin, A. (1969) *Science 164*, 1420−1421.
13. Damle, V. N., McLaughlin, M., and Karlin, A. (1978) *Biochem. Biophys. Res. Commun. 84*, 845−851.
14. Sullivan, D. A., and Cohen, J. B. (2000) *J. Biol. Chem. 275*, 12651−12660.
15. Zhong, W. G., Gallivan, J. P., Zhang, Y. N., Li, L. T., Lester, H. A., and Dougherty, D. A. (1998) *Proc. Natl. Acad. Sci. U.S.A. 95*, 12088−12093.
16. Cohen, J. B., Sharp, S. D., and Liu, W. S. (1991) *J. Biol. Chem. 266*, 23354−23364.
17. Grutter, T., Ehret-Sabatier, L., Kotzyba-Hibert, F., and Goeldner, M. (2000) *Biochemistry 39*, 3034−3043.
18. Kotzyba-Hibert, F., Kapfer, I., and Goeldner, M. (1995) *Angew. Chem., Int. Ed. 34*, 1296−1312.

19. Pedersen, S. E., Dreyer, E. B., and Cohen, J. B. (1986) *J. Biol. Chem. 261*, 13735−13743.
20. Blanton, M. P., Xie, Y., Dangott, L. J., and Cohen, J. B. (1999) *Mol. Pharmacol. 55*, 269−278.
21. White, B. H., Howard, S., Cohen, S. G., and Cohen, J. B. (1991) *J. Biol. Chem. 266*, 21595−21607.
22. Middleton, R. E., and Cohen, J. B. (1991) *Biochemistry 30*, 6987−6997.
23. Boyd, N. D., and Cohen, J. B. (1984) *Biochemistry 23*, 4023−4033.
24. White, B. H., and Cohen, J. B. (1988) *Biochemistry 27*, 8741−8751.
25. Chiara, D. C., and Cohen, J. B. (1997) *J. Biol. Chem. 272*, 32940−32950.
26. Blanton, M. P., and Cohen, J. B. (1992) *Biochemistry 31*, 3738−3750.
27. Schagger, H., and von Jagow, G. (1987) *Anal. Biochem. 166*, 368−379.
28. Pedersen, S. E., Sharp, S. D., Liu, W.-S., and Cohen, J. B. (1992) *J. Biol. Chem. 267*, 10489−10499.
29. Brauer, A. W., Oman, C. L., and Margolies, M. N. (1984) *Anal. Biochem. 137*, 134−142.
30. Sullivan, D., Chiara, D. C., and Cohen, J. B. (2002) *Mol. Pharmacol. 61*, 463−472.
31. Pedersen, S. E., and Cohen, J. B. (1990) *Proc. Natl. Acad. Sci. U.S.A. 87*, 2785−2789.
32. Middleton, R. E., Strnad, N. P., and Cohen, J. B. (1999) *Mol. Pharmacol. 56*, 290−299.
33. Pratt, M. B., Pedersen, S. E., and Cohen, J. B. (2000) *Biochemistry 39*, 11452−11462.
34. Gallagher, M. J., and Cohen, J. B. (1999) *Mol. Pharmacol. 56*, 300−307.
35. White, B. H., and Cohen, J. B. (1992) *J. Biol. Chem. 267*, 15770−15783.
36. Sigrist, H., Mühlemann, M., and Dolder, M. (1990) *J. Photochem. Photobiol. Biol. 7*, 277−287.
37. Dorman, G., and Prestwich, G. D. (1994) *Biochemistry 33*, 5661−5673.
38. Blanton, M. P., and Cohen, J. B. (1994) *Biochemistry 33*, 2859−2872.

BI0269815